# *Online estimation of MOSFET $R_{on}$ through Extended Kalman Filter*


Miguel Fernandez-Costales
*Power Supply Systems*
*University of Oviedo*
Gijon, Spain
fernandezcosmiguel@uniovi.es

Jose Antonio Fernandez-Alvarez
*Power Supply Systems*
*University of Oviedo*
Gijon, Spain
fernandezalvantonio@uniovi.es

Manuel Arias
*Power Supply Systems*
*University of Oviedo*
Gijon, Spain
ariasmanuel@uniovi.es

Pablo F. Miaja
*Power Supply Systems*
*University of Oviedo*
Gijon, Spain
fernandezmiapablo@uniovi.es

Jesus Oliver
*Power Management and Distribution*
*European Space Agency*
Noordwijk, The Netherlands
jesus.oliver@esa.int



***Abstract*—One of the key indicators of power converters degradation is an increase on the conduction resistance $R_{on}$ of the power switches. In this paper a method for estimating such increase, and thus converter degradation is presented. By means of utilizing an Extended Kalman Filter (EKF) it is possible to estimate this resistance increase from simple input and output voltage and current converter measurements. In this way, converter degradation can be detected, so actions can be taken to act accordingly. A prototype has been developed to perform online computation of the EKF.**



***Index Terms*—DC-DC converter, health monitoring, Extended Kalman Filter**


## I. Introduction

In critical power systems, such as those used in space systems, ensuring a high level of reliability is crucial. Any failure can jeopardize other systems or even the entire mission. Among all components, switching devices and capacitors are the most likely to fail [1], posing a risk to the overall reliability. However, in space applications self-healing capacitors are commonplace [2]. Therefore, determining whether a switching device is close to failure could prove more useful to guarantee the reliability. Before a failure, a MOSFET will experience a progressive increase in its $R_{on}$ resistance [3]. The limit before total failure is generally considered to be a 12% increase over the nominal value [4]. Adding additional circuits to measure $R_{on}$ is not desirable, as it would decrease reliability of the full system, in addition to increasing associated costs. Therefore, non-invasive methods that can estimate the $R_{on}$ value from signals normally used to control the converter are preferred. The Kalman filter and its variations for nonlinear applications [5], such as the extended Kalman filter (EKF) [6], are techniques that estimate the state of a dynamic system from noisy measurements. The procedure relies on the previous state value, and can be divided into two steps. First, a prediction step propagates the state estimation and its associated covariance matrix through the system's linearized model. Then, a correction step corrects the estimation upon receiving a new measurement of the states. Their fields of application are varied [7], [8]. Within power electronics, their use has been more restricted to motor control [9] or to determine the state of charge of batteries [10]. They have also been used as estimators when sensor use is difficult [11]. Applications focused on parameter estimation in converters have been proposed in [12] and [13]. $R_{on}$-based estimates are made in [14], but using the averaged model and open-loop converters. Reference [15] provides an overview of several methods to determine the Remaining Useful Lifetime (RUL) of the converter, although the shown methods rely on actual measurements and they are more invasive than the ones used in this paper.

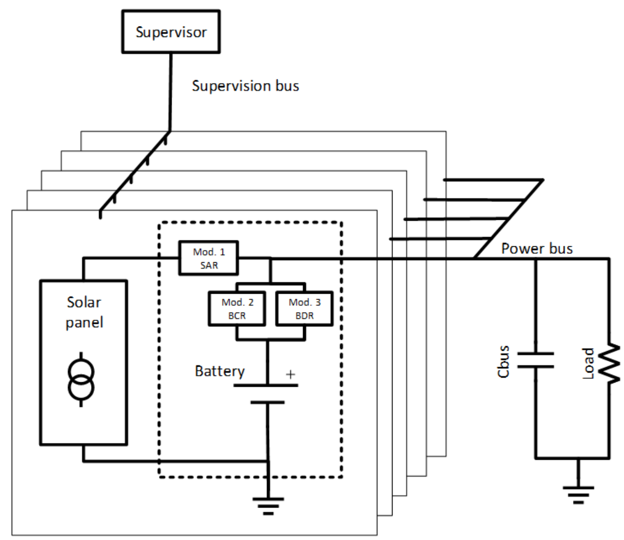


Fig. 1. Satellite power architecture

The case study of this work is a modular satellite power system, where several parallel converters regulate the bus voltage [16], following the block diagram in Fig 1. Each of these converters acts as a current source. A main supervisor decides how much power is provided by each converter, so it is possible to adjust these levels based on the detected degradation of the converters. In this way, a prognostic method is implemented to predict when one of the modules has undergone excessive degradation based on the estimation of the $R_{on}$ resistance value of the switching elements, allowing less power to be drawn from the module and extending its useful lifetime. Although it is a very specific application, a general methodology is proposed, and the estimation system could be adapted to almost any controlled DC/DC converter.

This article is organized into the following sections. Section II analyzes the operation of the boost converter used. Section III focuses on the application of the extended Kalman filter to said converter. Section IV collects the experimental results obtained. Finally, Section V includes the main conclusions of this work.

## II. Application to a boost converter

The power converter analyzed in this paper is the boost converter, following the schematics in Fig.2. In this paper the use case for this topology is a modular space power system where several converters regulate the main bus. Then the output voltage $V_o$ is defined as a constant voltage source. All these converters are digitally current controlled adjusting the duty cycle $d$ so a sample of the current through the inductor $I_L$ matches a certain value, defined as $I_{ref}$. By wisely taking this sample at the middle of the switching period this sample corresponds to the average current through the inductor [17]. In this paper the EKF has two states, which are related to each other. One of them could not be measured, only estimated thus it is a hidden state. This will be the parasitic resistance $r_l$. This resistance models all the parasitic resistances of the circuit which affect the current flow through the inductor.Therefore, it is affected by other parasitic elements in the circuit, such as

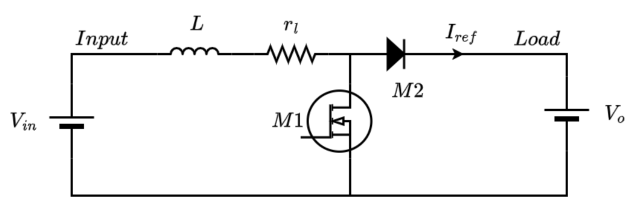


Fig. 2. Boost converter schematics

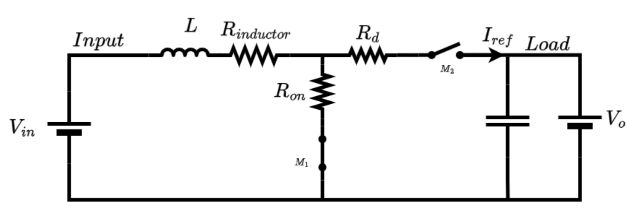


Fig. 3. Equivalent circuit to showcase the effects of $R_{on}$ on $r_l$

the inductor series resistance $R_{inductor}$ or the diode resistance $R_D$, as it is shown in Fig 3. By taking into consideration these two parasitic resistances, apart from the $R_{on}$, the effects of the latter over $r_l$ can be considered as

$$r_l = (R_{inductor} + R_{on}) \cdot d + (R_{inductor} + R_D) \cdot (1 - d) \quad (1)$$

where $d$ is the duty cycle applied at the given switching period. The other state could be measured, therefore this is an observable state. This state is based in the current ripple through the inductor. An additional sample of the inductor current, defined as $I_{rip}$, is taken during the same switching cycle $T_s$ as the one used to control the inductor current $I_{ref}$. The difference between $I_{rip}$ and $I_{ref}$ results in the observable state $\Delta i$, which will be used by the EKF to estimate $r_l$. The converter that has been studied has two switching states, one when $M_1$ is conducting, during $d \cdot T_s$, and a second one when $M_1$ is off, during $(1-d) \cdot T_s$. Thus, a system state space description could be defined as

$$\dot{\Delta i} = \begin{cases} \frac{V_{in}}{L} - \frac{r_l}{L} \cdot \Delta i - \frac{r_l}{L} \cdot I_{ref} & \text{if } 0 < t < d \cdot T_s \\ \\ \frac{V_{in}}{L} - \frac{V_o}{L} - \frac{r_l}{L} \cdot \Delta i - \frac{r_l}{L} \cdot I_{ref} & \text{if } d \cdot T_s < t < T_s \end{cases} \quad (2)$$

This state space description can be utilized by the EKF in the state prediction for the next switching cycles. in this description $V_{in}$,$V_o$ and $I_{ref}$ are the inputs to the system.

### A. State propagation

As aforementioned, the system consists of two states: an observable one, $\Delta i$, defined as the difference between $I_{ref}$ and $I_{rip}$, which is used as baseline for the prediction of the other state, in this case unobservable, $r_l$. Changes in $\Delta i$, without changes in the inputs ($V_{in}$,$V_o$ and $I_{ref}$), will show that there has been a change in $r_l$. This unobserved state is considered an augmented state and has no dynamics, hence $\dot{r_l} = 0$.

To determine how $\Delta i$, evolves through the next switching period, it is propagated one switching cycle, following

$$\Delta i(T_s) = e^{\frac{-r_l}{L}T_s} \cdot \Delta i(0) + \int_0^{T_s} e^{\frac{-r_l}{L}(T_s-\tau)} \cdot B(\tau) \cdot \begin{bmatrix} V_{in} \\ V_{out} \\ I_{ref} \end{bmatrix} d\tau \quad (3)$$

As it can be seen in Fig 4, if $I_{rip}[n-1]$ is taken as a reference it must be propagated through the different switching states of the converter. This allows to calculate the evolution of $\Delta i[n-1]$ at the switching state changes at $t_1$ and $t_3$. Then, the temporal evolution at the next sample ( which takes place at $t_4$) is

$$\Delta i(t_1) = e^{\frac{-r_l}{L}t_1} \cdot \Delta i(0) + \left[\frac{V_{in}}{r_l} - I_{ref} - \frac{V_o}{r_l}\right] \cdot \left[1 - e^{\frac{-r_l}{L}t_1}\right] \quad (4)$$

$$\Delta i(t_3) = e^{\frac{-r_l}{L}(t_3-t_1)} \cdot \Delta i(t_1) + \left[\frac{V_{in}}{r_l} - I_{ref}\right] \cdot \left[1 - e^{\frac{-r_l}{L}(t_3-t_1)}\right] \quad (5)$$

$$\Delta i(t_4) = e^{\frac{-r_l}{L}(t_4-t_3)} \cdot \Delta i(t_3) + \left[\frac{V_{in}}{r_l} - I_{ref} - \frac{V_o}{r_l}\right] \cdot \left[1 - e^{\frac{-r_l}{L}(t_4-t_3)}\right] \quad (6)$$

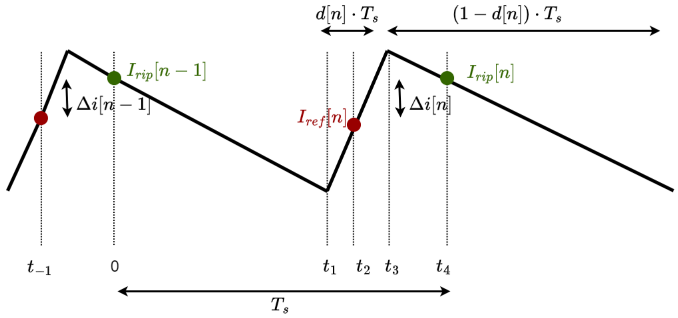


Fig. 4. Inductor current sampling

Given the approximation $e^{\frac{-r_l}{L}}T_s \approx (1 - \frac{r_l}{L}T_s)$

$$\begin{aligned}\Delta i(t_4) &= \left(1 - \frac{r_l}{L}t_4\right)\Delta i(0) \\ &+ t_4\left(\frac{V_{in}}{L} - I_{ref}\frac{r_l}{L} - \frac{V_o}{L}\right) + (t_3 - t_1)\frac{V_o}{L}\end{aligned} \tag{7}$$

Considering now that $t_4 = T_s$ and that $t_3 - t_1 = d \cdot T_s$,

$$\begin{aligned}\Delta i(T_s) &= \left(1 - \frac{r_l}{L}T_s\right) \cdot \Delta i(0) \\ &+ \left(\frac{V_{in}}{L} + \frac{V_o}{L}(d-1)\right) \cdot T_s - I_{ref} \cdot \frac{r_l}{L}T_s\end{aligned} \tag{8}$$

(8) provides the value of the next sample of $\Delta i[n]$, which is part of the state transition function $F(X[n], U[n])$.

## III. EKF DEVELOPMENT

Using the previous equations, all the parameters needed to compute the EKF can be calculated. The states are

$$X[n] = \begin{bmatrix} \Delta i[n] \\ r_l[n] \end{bmatrix} \tag{9}$$

The input control variables can be reformulated into

$$U[n] = \begin{bmatrix} \Delta V[n] \\ I_{ref}[n] \end{bmatrix} \tag{10}$$

where

$$V[n] = V_{in}[n] - (1 - d[n]) \cdot V_o[n] \tag{11}$$

The state transition function $F(X[n], U[n]) = X[n+1]$ is

$$F(X[n], U[n]) = \begin{bmatrix} \left(1 - \frac{r_l[n]}{L}T_s\right)\Delta i[n] + \left(V[n]\frac{T_s}{L}\right) - I_{ref}[n]\frac{r_l}{L}T_s \\ r_l[n] \end{bmatrix} \tag{12}$$

The measurement matrix $H(X[n])$ represents how the state is seen by the measurement sensors. In this case

$$H(X[n]) = \Delta i[n] \tag{13}$$

As the system is nonlinear, the state transition function is linearized around the previous state. To do that, the Jacobian matrix is computed

$$J_F[n] = \frac{\delta F[n]}{\delta X[n]} = \begin{bmatrix} \frac{\delta \Delta i[n]}{\delta \Delta i[n]} & \frac{\delta \Delta i[n]}{\delta r_l[n]} \\ \frac{\delta r_l[n]}{\delta \Delta i[n]} & \frac{\delta r_l[n]}{\delta r_l[n]} \end{bmatrix} \tag{14}$$

In a similar way, the Jacobian matrix of the measurement matrix is

$$J_H[n] = \frac{\delta H[n]}{\delta X[n]} = \begin{bmatrix} \frac{\delta \Delta i[n]}{\delta \Delta i[n]} & \frac{\delta \Delta i[n]}{\delta r_l[n]} \end{bmatrix} \tag{15}$$

These Jacobian matrices are used to predict the state covariance.

The process error covariance matrix $Q$, and the measurement error covariance matrix $R$, model the system noise. $Q$ indicates the error in the model that represents the dynamic evolution of the system. These values are calculated empirically [18] [19]. It is, in this case

$$Q = \begin{bmatrix} Q_{\Delta i \Delta i} & Q_{\Delta i r_l} \\ Q_{r_l \Delta i} & Q_{r_l r_l} \end{bmatrix} \tag{16}$$

The measurement error covariance matrix R models the noise present in the sensors. Just as with $Q$, it is obtained through calibration processes. It is

$$R = R_0 \tag{17}$$

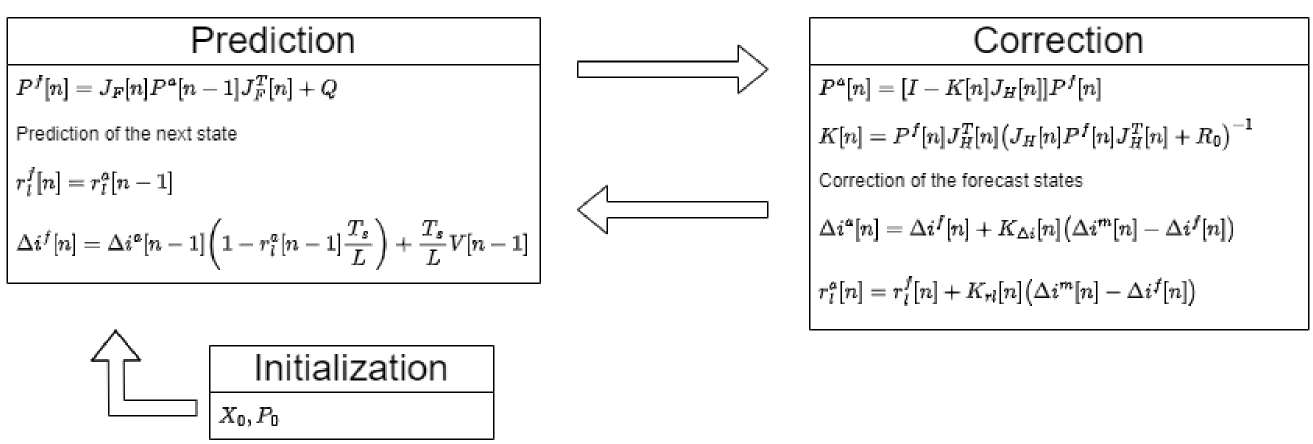


Fig. 5. Kalman filter algorithm block diagram.

where $R_0$ is the sensor error.

The covariance matrix $P$ indicates the confidence in the state estimates of the EKF at a given moment. This matrix is updated in each iteration during the prediction stage, incorporating the process error (matrix $Q$). In the correction stage, $P$ is further adjusted by adding information from the measurements through the Kalman gain. The Kalman gain determines how much weight is given to the measurements with respect to the prediction.

In this way, the iterative process of the EKF can be initiated, consisting of: initialization, prediction, and correction of values. Fig 5 shows the iterative process of this algorithm.

- *Initialization*
  The EKF requires an estimate of the initial states $X_0$ as well as the covariance matrix $P_0$ that indicates the certainty of this estimate. These values can be obtained by simulation. Then,

$$X_0 = \begin{bmatrix} \Delta i_0 \\ r_{l0} \end{bmatrix} \tag{18}$$

$$P_0 = \begin{bmatrix} P_{\Delta i \Delta i_0} & P_{\Delta i r_{l0}} \\ P_{r_l \Delta i_0} & P_{r_l r_{l0}} \end{bmatrix} \tag{19}$$

  The EKF aims to predict the state values $\Delta i^f[n]$ and $r_l^f[n]$ from the corrected samples of the previous cycle $\Delta i^a[n-1]$ and $r_l^a[n-1]$. Since $\Delta i^m[n] = I_{ref}[n] - I_{rip}[n]$, this state will be used to correct the predictions with the Kalman gain. In this study, it is assumed that the EKF operates in a steady state, which implies that the input variables ($V_o, I_{ref}, V_{in}$) do not change during a switching period. The state $\Delta i$ has a dynamic behavior that depends on $V_{in}, V_o, I_{ref}$, duty cycle $d$, and state $r_l$.
- *Prediction*
  In this step, the EKF makes predictions of the states $\Delta i^f[n]$ and $r_l^f[n]$ and the covariance matrix $P^f[n]$, from the matrix of the corrected states of the previous instant, where

$$\begin{aligned} \Delta i^f[n] &= \Delta i^a[n-1] \cdot \left(1 - r_l^a[n-1] \cdot \frac{T_s}{L}\right) \\ &+ \frac{T_s}{L} V[n-1] - I_{ref}[n-1] \frac{T_s}{L} r_l^a[n-1] \end{aligned} \tag{20}$$

$$r_l^f[n] = r_l^a[n-1] \tag{21}$$

  The prediction of the covariance matrix is made from the Jacobian $J_F[n]$, where

$$P^f[n] = J_F[n] \cdot P^a[n-1] \cdot J_F^T[n] + Q \tag{22}$$

- *Correction*
  In this stage, the Kalman gain is calculated from the predicted covariance matrix $P^f[n]$. Thus,

$$\begin{aligned} K[n] = \begin{bmatrix} K_{\Delta i}[n] \\ K_{rl}[n] \end{bmatrix} &= P^f[n] \cdot J_H^T[n] \cdot \\ &\left(J_H[n] \cdot P^f[n] \cdot J_H^T[n] + R_0\right)^{-1} \end{aligned} \tag{23}$$

  The values of the covariance matrix $P^a[n]$ are updated to correct the estimated values with measurement information through

$$P^a[n] = (I - K[n] \cdot J_H[n]) \cdot P^f[n] \tag{24}$$

  In this stage, the mean of the states is also corrected using the Kalman gain and the difference between the measured and predicted values. Therefore,

$$\Delta i^a[n] = \Delta i^f[n] + K_{\Delta i}[n] \cdot (\Delta i^m[n] - \Delta i^f[n]) \tag{25}$$

$$r_l^a[n] = r_l^f[n] + K_{rl}[n] \cdot (\Delta i^m[n] - \Delta i^f[n]) \tag{26}$$

The description of the correction of the states provides the framework which updates the unobservable state $r_l$. This one is updated through the corrections between the prediction and the measurements of state $\Delta i$.

## IV. Experimental Results

### A. EKF implementation

Making use of the Texas Instruments C2000 Microcontroller Blockset, a version of the EKF was implemented on Simulink that allows it to be programmed onto the controller, along the control stage of the DC/DC converter. This provides an online $r_l$ estimation system. Table I gathers all the main components of this implementation, requiring very few resources and resulting in an adequate solution with a compact computational cost. The Simulink block diagram is depicted in Fig 6.

TABLE I
EKF implementation size

| Operation | Value |
|---|---|
| Additions | 23 |
| Registers | 8 |
| Multiplications | 19 |
| Divisions | 2 |

### B. Results

The validation was carried out with a custom platform based on a boost converter. Input and output voltage values, duty cycle, and inductor currents are captured. Additionally, this platform includes additional circuitry to measure the voltages and currents of the switching MOSFET, that allow to calculate the $R_{on}$. This value is compared with the EKF estimation. All these data are acquired using a Texas Instruments TMS320F28379 DSP, which is also responsible for controlling the converter. In this case, average current mode control

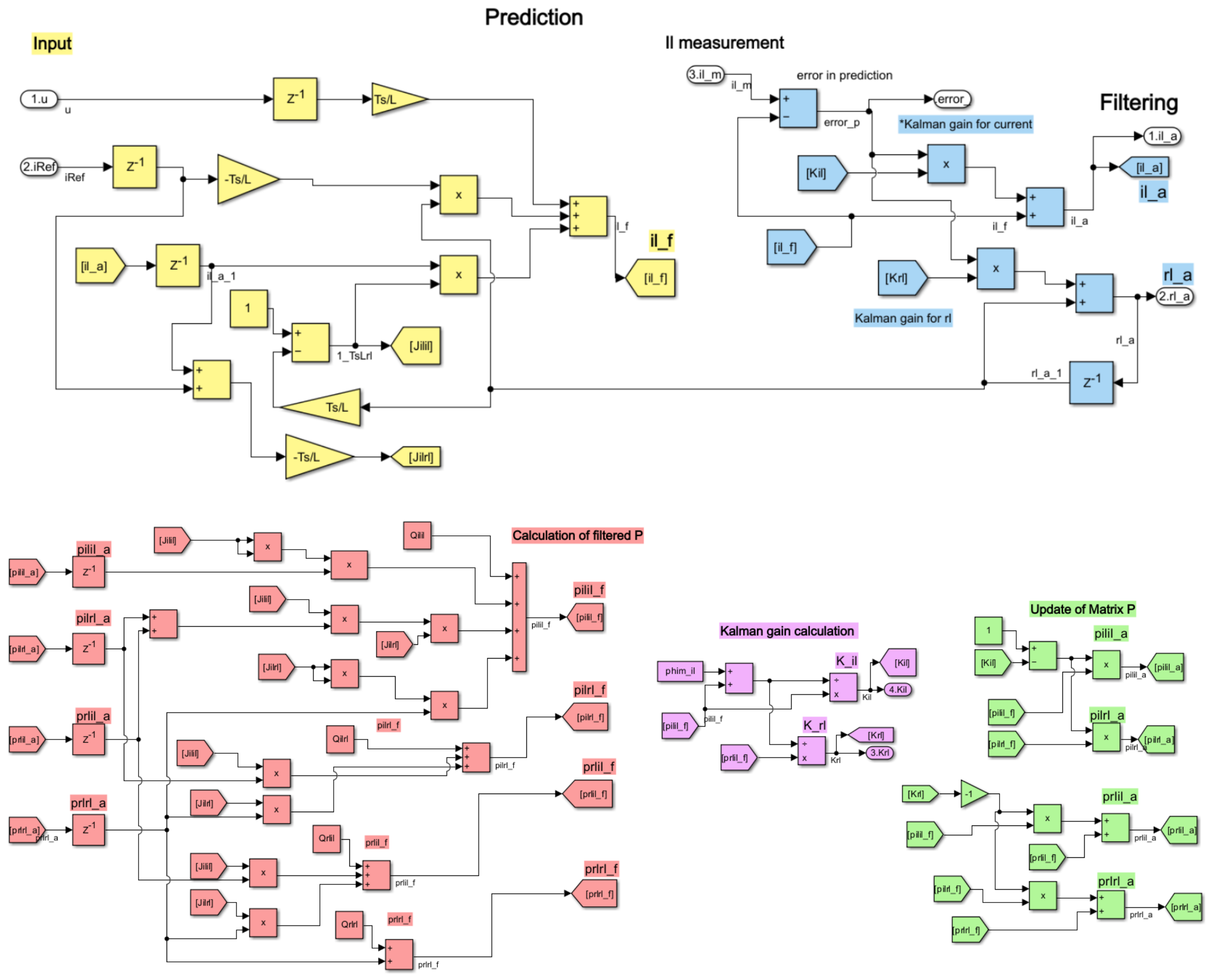


Fig. 6. Kalman filter algorithm Simulink block diagram.

is performed, where the inductor reference current is fixed to 2.5 A. Current sensing is performed using Hall sensors, specifically the ACS730 models from Allegro Microsystems, with a bandwidth of 1 MHz. The block diagram of the experimental implementation is depicted in Fig 7, while the experimental setup is shown in Fig 8. The selected MOSFET is the SPP20N60S5 with an $R_{on}$ of 0.19 $m\Omega$. A switching frequency of 10 kHz was chosen to avoid data losses during data transmission to the PC with MATLAB which records the data for representation. This computer is also used to program the DSP. Other parameters of interest used in the experimentation are collected in Table II.

Apart from samples of the inductor current, $I_{ref}$ used for the current control loop, which determines $d$, and $I_{rip}$ for the EKF, samples of $V_{in}$ and $V_o$ are also taken for the EKF. Additionally the DSP also takes measurements of the current through the MOSFET and its drain to source voltage while on. These data are used by the DSP to calculate the prediction of $r_l$, $r_{l\_est}$, which is then sent to an external PC with Simulink along

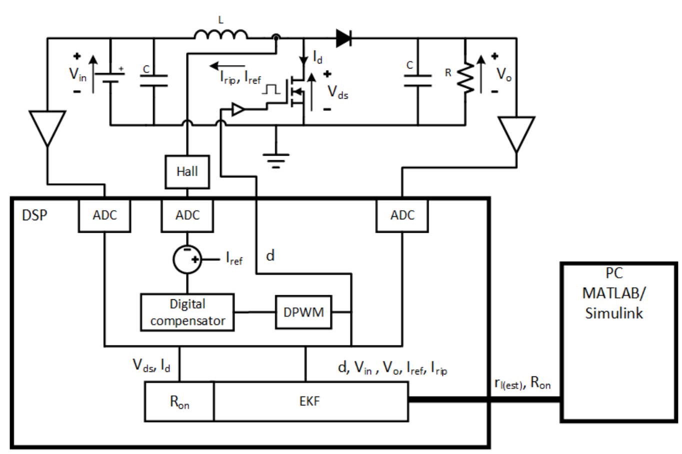


Fig. 7. Setup block diagram.

with the switching MOSFET measured resistance $R_{on}$. This is made for visualizing data in real time. All the processing is

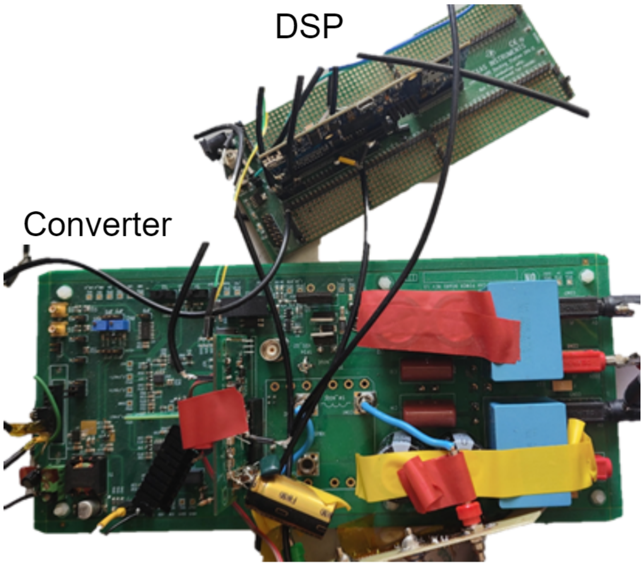


Fig. 8. Experimental setup.

done by the DSP.

Fig. 9 shows the data used as input for the EKF. It includes a fixed output voltage $V_o$ of 30 V, an input voltage $V_{in}$ ranging from 15-17 V, the current samples $I_{ref}$ and $I_{rip}$, with $I_{ref}$ being the reference current for the control, and duty cycle $d$. With these data, the prediction is made. Fig. 10 shows the estimated difference between the two current samples through the inductor $\Delta i_{(est)}$ versus the real value $\Delta i$, and the augmented state $r_{l(est)}$ corresponding to the estimated parasitic resistance of the system, versus the real $R_{on}$. The changes in $R_{on}$ were artificially introduced by lowering the driving voltage of the MOSFET between 17 $V$ for the lower $R_{on}$ values and 12 $V$ for the higher ones. The change in the driving voltage takes place approximately at time $t = 35$ $s$. It can be seen how $d$ increases a little bit to keep the current constant in spite of the increased resistance. Figure 11 focuses in more detail on the differences between the measured resistance, $R_{on}$, and the predicted one, $R_{on\_EKF}$ based on the predicted $r_l$ and separating the different elements, as per (1). It can be seen that during the transient, the EKF doesn't have enough time to converge, providing a different value estimation, which then diminishes once the final resistance value has reached.

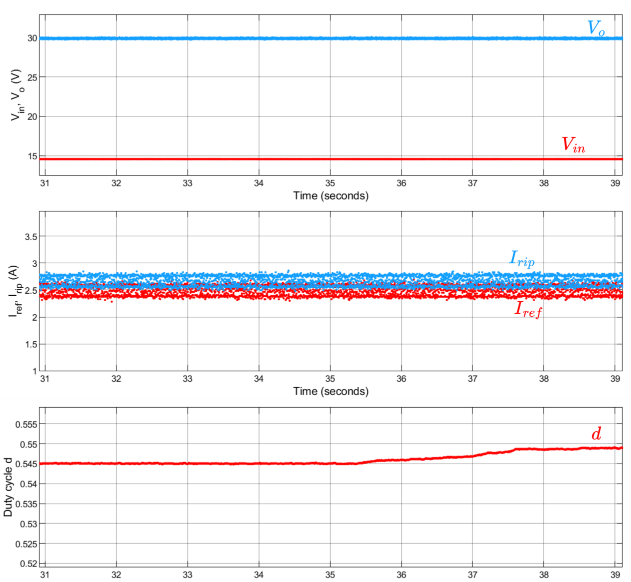


Fig. 9. EKF input values.

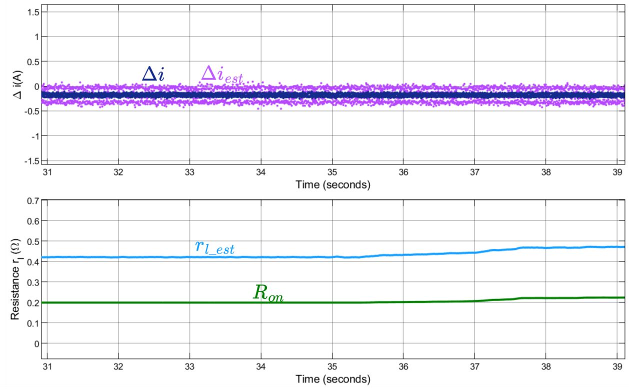


Fig. 10. EKF output, comparison with measurements.

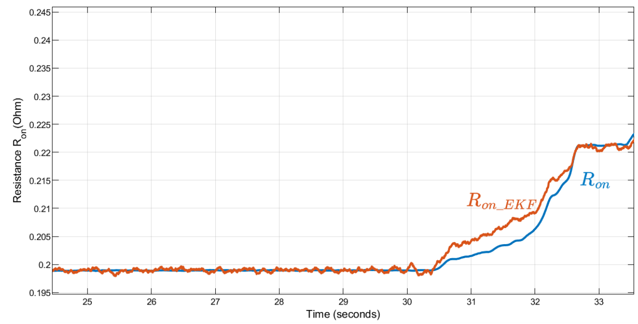


Fig. 11. Output of the EKF: $R_{on}$ estimation comparison with measurement.

## V. Conclusions

In this work, a method is presented to predict the conduction resistance $R_{on}$ of switching MOSFETs in power converters with the objective of preventing catastrophical failures and extending their useful lifetime. This method is based on the use of an extended Kalman filter, providing a feasible solution that doesn't require any invasive measurement. By measuring input voltage $V_{in}$, output voltage $V_o$, inductor current at two samples within the same switching period $I_{ref}$ and $I_{rip}$, and duty cycle $d$, it is possible to obtain a prediction of the parasitic resistance $r_l$, which can then be extrapolated to the detection of an increase in conduction resistance $R_{on}$ of the switching MOSFET. The validation of this method has been carried out experimentally using a boost converter with 15 V input voltage and 30 V output voltage. By comparing the augmented output of the extended Kalman filter, which represents the parasitic

TABLE II
PARAMETERS AND VALUES

| Parameter | Value |
|---|---|
| $V_{in}$ | 15 V |
| $V_o$ | 30 V |
| $I_{ref}$ | 2.5 A |
| $f_s$ | 10 kHz |
| $L$ | 275 $\mu H$ |
| $\Delta R_{on}$ | 10% |

resistance of the circuit $r_l$, with the measured $R_{on}$ of the switching MOSFET it has been shown that changes in $R_{on}$ value, artificially increased by changing the driver's supply voltage, ara properly tracked by the EKF output. The EKF has been implemented on the DSP controlling the boost converter. By allowing it to be implemented on the controller, there is no need for external data processing. The results show it is possible to detect an increase in the conduction resistance of the switching element, that is, the $R_{on}$ of the switching MOSFET, which is sufficient to determine premature aging in the component.

## ACKNOWLEDGMENT

This work has been funded by the Spanish government through grant PID2021-127707OB-C21, by the Principality of Asturias through the Severo Ochoa grant BP21-207 and throug the European Space Agency (ESA) project Health monitoring of Digitally Controlled Flexible Converters ESA Contract No. 4000129432/19/NL/AS/hh.

## REFERENCES

[1] L. Ferreira Costa and M. Liserre, "Failure Analysis of the dc-dc Converter: A Comprehensive Survey of Faults and Solutions for Improving Reliability," IEEE Power Electron. Mag., vol. 5, no. 4, pp. 42–51, Dec. 2018, doi: 10.1109/MPEL.2018.2874345.

[2] A. Teverovsky, "Breakdown and Self-healing in Tantalum Capacitors," IEEETrans. Dielect. Electr. Insul., vol. 28, no. 2, pp. 663–671, Apr. 2021, doi: 10.1109/TDEI.2020.009240.

[3] J. R. Celaya, A. Saxena, S. Saha, V. Vashchenko, and K. Goebel, "Prognostics of power MOSFET," in 2011 IEEE 23rd International Symposium on Power Semiconductor Devices and ICs, San Diego, CA, USA: IEEE, May 2011, pp. 160–163. doi: 10.1109/ISPSD.2011.5890815.

[4] S. Dusmez, M. Bhardwaj, L. Sun, and B. Akin, "In Situ Condition Monitoring of High-Voltage Discrete Power MOSFET in Boost Converter Through Software Frequency Response Analysis," IEEE Trans. Ind. Electron., vol. 63, no. 12, pp. 7693–7702, Dec. 2016, doi: 10.1109/TIE.2016.2595482.

[5] Simon, D. Kalman Filtering with State Constraints: A Survey of Linear and Nonlinear Algorithms. IET Control Theory and Applications, 4, 1303–1318. issn: 1751-8644, 1751-8652 (Aug. 1, 2010).

[6] Senne, K. Stochastic Processes and Filtering Theory. IEEE Transactions on Automatic Control 17, 752–753. issn: 1558-2523 (Oct. 1972).

[7] B. Chen, W.-A. Zhang, and L. Yu, "Distributed Finite-Horizon Fusion Kalman Filtering for Bandwidth and Energy Constrained Wireless Sensor Networks," IEEE Trans. Signal Process., vol. 62, no. 4, pp. 797–812, Feb. 2014, doi: 10.1109/TSP.2013.2294603.

[8] M. Lipka, E. Sippel, and M. Vossiek, "An Extended Kalman Filter for Direct, Real-Time, Phase-Based High Precision Indoor Localization," IEEE Access, vol. 7, pp. 25288–25297, 2019, doi: 10.1109/ACCESS.2019.2900799.

[9] E. Zerdali and M. Barut, "The Comparisons of Optimized Extended Kalman Filters for Speed-Sensorless Control of Induction Motors," IEEE Trans. Ind. Electron., vol. 64, no. 6, pp. 4340–4351, Jun. 2017, doi: 10.1109/TIE.2017.2674579.

[10] Mastali, M. et al. Battery State of the Charge Estimation Using Kalman Filtering. Journal of Power Sources 239, 294–307. issn: 03787753 (Oct. 2013).

[11] Haadi, K., Rajaei, A., Shahparasti, M. and Rahideh, A. Sensorless Voltage Observer for a Current-Fed High Step-Up DC-DC Converter Using Extended Kalman Filter. Electronics 9, 2066. issn: 2079-9292 (Dec. 4, 2020).

[12] Missailidis, P., Armstrong, M., Gadoue, S. and Ahmeid, M. Parameter Estimation of a DC-DC Converter Using a Kalman Filter Approach in 7th IET International Conference on Power Electronics, Machines and Drives (PEMD 2014) 7th IET International Conference on Power Electronics, Machines and Drives (PEMD 2014) (Institution of Engineering and Technology, Manchester, UK, 2014), 0339–0339. isbn: 978-1-84919-815-8.

[13] Beccuti, A. G., Mariethoz, S., Cliquennois, S., Wang, S. and Morari, M. Explicit Model Predictive Control of DC–DC Switched-Mode Power Supplies With Extended Kalman Filtering. IEEE Transactions on Industrial Electronics 56, 1864–1874 (2009).

[14] Alyakhni, A., Al-Mohamad, A. and Hoblos, G. Joint Estimation of MOSFET Degradation in a DC-DC Converter Using Extended Kalman Filter in 2019 4th Conference on Control and Fault Tolerant Systems (SysTol) 2019 4th Conference on Control and Fault Tolerant Systems (SysTol) (IEEE, Casablanca, Morocco, Sept. 2019), 319–324. isbn: 978-1-72810-380-8.

[15] Kathribail, P. S. and Vijayakumar, T. Comprehensive Study of MOSFET Degradation in Power Converters and Prognostic Failure Detection Using Physical Model. Journal of The Institution of Engineers (India): Series B 104, 305–317. issn: 2250-2114 (Feb. 1, 2023).

[16] Zumel, P. et al. Digital Control for a Modular System of DC/DC Converters for Primary Distribution System in 2023 13th European Space Power Conference (ESPC) 2023 13th European Space Power Conference (ESPC) (IEEE, Elche, Spain, Oct. 2, 2023), 1–6. isbn: 9798350328998.

[17] L. Corradini, D. Maksimović, P. Mattavelli, and R. Zane, "Digital control of high-frequency switched-mode power converters." Hoboken, New Jersey: IEEE, John Wiley & Sons Inc, 2015.

[18] J. Valappil and C. Georgakis, "Systematic estimation of state noise statistics for extended Kalman filters," AIChE Journal, vol. 46, no. 2, pp. 292–308, Feb. 2000, doi: 10.1002/aic.690460209.

[19] R. Bos, X. Bombois, and P. M. J. Van Den Hof, "DESIGNING A KALMAN FILTER WHEN NO NOISE COVARIANCE INFORMATION IS AVAILABLE," IFAC Proceedings Volumes, vol. 38, no. 1, pp. 1275–1280, 2005, doi: 10.3182/20050703-6-CZ-1902.00213.